Non-neutral ion plasmas and crystals, laser cooling, and atomic clocks*

J. J. Bollinger† and D. J. Wineland
Time and Frequency Division, NIST, Boulder, Colorado 80303

Daniel H. E. Dubin
Department of Physics, University of California at San Diego, La Jolla, California 92093

(Received 3 November 1993; accepted 4 January 1994)

Experimental work which uses Penning and Paul traps to confine non-neutral ion plasmas is discussed. Penning traps use a static uniform magnetic field and a static electric field to confine ions. The Paul trap uses the ponderomotive force from inhomogeneous radio-frequency fields to confine ions to a region of minimum field strength. In many atomic physics experiments, these traps are designed to produce a harmonic restoring force for small numbers of stored ions ($<10^4$). Under these conditions and at low temperatures, both traps produce plasmas with simple shapes whose mode properties can be calculated exactly. Laser cooling has been used to reduce the temperature of trapped ions to less than 10 mK with ion spacings less than 20 μm. At such temperatures and interion spacings, the Coulomb potential energy between nearest neighbor ions is greater than the ion thermal energy and the ions exhibit spatial correlations characteristic of a liquid or crystal. Laser beams also apply a torque which, by changing the plasma angular momentum, changes the plasma density. Atomic clocks are an important application of ion trap plasmas. Better control of the plasma dynamics will reduce fluctuations in the relativistic time dilation, yielding better clocks.

I. INTRODUCTION

Non-neutral plasmas consist of a collection of charged particles with a single sign of charge. Over the past 40 years non-neutral plasmas have been carefully studied in a variety of experiments.[1,2] Many of these studies involved intense electron or ion beams which are used, for example, in advanced high current accelerators or in coherent radiation generation.[1,2] This article will review a very different type of non-neutral plasma: a three-dimensionally confined, low-energy non-neutral plasma that consists of a single charged species. The discussion will concentrate on pure ion plasmas and their connection to pure electron plasmas. Much of the work discussed here is related to current experiments in atomic physics. For example, small non-neutral ion plasmas are being used to make high-resolution spectroscopic measurements on ions. These high resolution measurements could potentially lead to a new generation of atomic clocks.[3–6]

Pure ion or electron non-neutral plasmas exhibit some of the same properties as neutral plasmas. For example, they exhibit collective effects such as plasma waves and shielding on the scale of a Debye length.[1] However, there are notable differences. For example, the confinement of non-neutral plasmas is much better than the confinement of neutral plasmas. In some cases, confinement times of many hours can be achieved.[7] The confinement time can be sufficiently long that the plasma evolves into a state of thermal equilibrium.[8] Another unique property of non-neutral plasmas is that they can be cooled. If a neutral plasma is cooled, the positive ions will eventually recombine with the negative electrons. In a pure ion plasma there are no free electrons to recombine with the ions. These plasmas can be cooled to cryogenic temperatures, where strong correlation effects become important. With electrons, cooling has been accomplished through electron cyclotron radiation[9,10] and coupling of the electrons' motion to external circuits.[11,12] Momentum transfer from a laser beam has been used to efficiently cool non-neutral ion plasmas (laser cooling).[13]

The two most common types of traps for atomic and molecular ion experiments are the Penning trap, named after Penning,[14–17] and the radio frequency (RF) or Paul trap, named after Wolfgang Paul.[15–18] The Penning trap confines particles by superimposing an electrostatic well along the direction of the field lines of a homogeneous magnetic field. A Paul trap confines charged particles by the ponderomotive force provided by inhomogeneous oscillating electric fields. A configuration often used in atomic ion experiments is one where the electric potential is quadratic, arising from electrodes, as shown in Fig. 1. For this case, both traps can be described by superimposing a quadrupole electric potential and a magnetic field

$$\phi_T(r,z)=\frac{U_0+V_0\cos\omega_{\rm rf}t}{r_T^2+2z_T^2}(2z^2-r^2),\quad \mathbf{B}=B\hat{z}, \qquad (1)$$

where r and z are cylindrical coordinates and r_T and z_T are characteristic internal dimensions of the trap (Fig. 1). For the Penning trap, $V_0=0$, and for the Paul trap, $V_0\neq 0$ and $B=0$. Hybrid traps have also been studied where U_0, V_0, and B are all nonzero.[19,20] In Sec. II we show that an RF trap plasma is a special case of a Penning-trap plasma. Therefore much of the discussion throughout this review centers on Penning traps.

Elongated Penning traps with cylindrical electrodes replacing the electrodes of the quadrupole trap shown in

*Paper 5RV1, Bull. Am. Phys. Soc. **38**, 1984 (1993).
†Invited speaker.

 1070-664X/94/1(5)/1403/12/$6.00

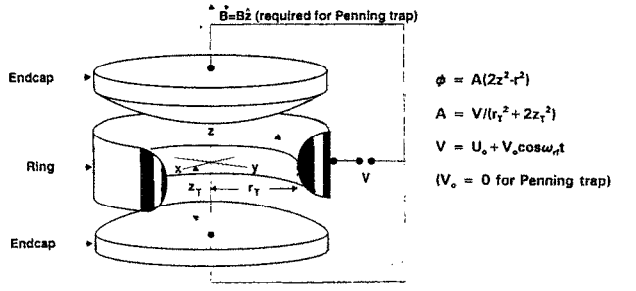

FIG. 1. Common electrode configuration used for Penning and Paul traps in atomic physics experiments. The quadratic trap potential is a consequence of the shape of the electrodes, which are hyperboloids of revolution [and therefore equipotentials of the potential in Eq. (1)]. We neglect the distortion of the potential from the effects of truncation and holes in the electrodes.

Fig. 1 have been used extensively in electron non-neutral plasma experiments by the group at the University of California at San Diego (UCSD).[10,21] Linear Paul traps have been used in some experiments to study the collective properties of stored ions.[22,23] These traps are composed of a ponderomotive potential in two dimensions (like a quadrupole mass analyzer) and an electrostatic well in the third dimension. [For example, in Eq. (1), we let $r^2 \to 2x^2$ and $r_T^2 \to 2x_T^2$, which provides a ponderomotive well in the x-z plane. On this potential we superimpose an electrostatic well along y to provide trapping in three dimensions.]

Penning and Paul traps are useful for high resolution spectroscopy and its application to atomic clocks. Atomic clocks generate time intervals by counting the cycles of an oscillator which is made synchronous with a particular transition frequency in an atom or ion. Ion traps have some advantages over other techniques for spectroscopy: (1) Atomic ion storage times can be very long, so the resolution of the transitions can be very high—linewidths less than 0.001 Hz have been observed.[4] (2) The ions are often stored under high-vacuum conditions, which suppresses the systematic frequency shifts due to collisions with background gas. (3) The average velocity of stored ions is 0; so the first-order Doppler shift vanishes. Laser cooling reduces substantially the second-order Doppler shift (relativistic time dilation). Inaccuracies of atomic clocks based on stored ions may eventually be less than 1 part in 10^{18} (Ref. 4).

The main disadvantage of using stored ions in atomic clocks (as opposed to neutral atom clocks) is that the densities of ions are relatively low because of Coulomb repulsion between ions. This means that the signal-to-noise ratio is relatively small. Nevertheless, sensitive detection techniques[24] have been realized with stored ions, and the signal-to-noise ratio can be limited only by the fundamental quantum fluctuations of the measurements.[25]

II. THERMAL EQUILIBRIUM

The long confinement times of non-neutral plasmas enable the plasma to evolve to a state of confined thermal equilibrium.[8] In the RF trap, the ions are confined in three dimensions by the ponderomotive fields. In the Penning trap, the ions are confined in the axial direction by the static potentials on the trap electrodes. However, the long-term radial confinement in a Penning trap is less obvious. To understand this confinement[26] it is useful to consider the canonical angular momentum about the trap's symmetry axis

$$P_\theta = \sum_j \left(m v_{\theta_j} + \frac{q}{c} A_\theta(r_j) \right) r_j, \tag{2}$$

where r and θ are cylindrical coordinates; m, v, and q are the ion mass, velocity, and charge; and the sum is over all ions. The vector potential $A_\theta(r) = Br/2$ is for a uniform axial magnetic field. The first term in Eq. (2) is the mechanical angular momentum of the ions. The second term can be associated with the angular momentum of the field. In most Penning-trap experiments, the mechanical angular momentum is small compared to the field angular momentum and Eq. (2) can be approximated as

$$P_\theta \simeq \frac{qB}{2c} \sum_j r_j^2. \tag{3}$$

Equation (3) places a very powerful constraint on the plasma. To the extent that the trap is azimuthally symmetric, P_θ is constant and the mean square radius of the plasma is conserved. This constraint is not valid for neutral plasmas. In a neutral plasma an electron and an ion can move to the wall together and still conserve the canonical angular momentum.

In practice, Penning traps have been constructed with sufficient symmetry to give non-neutral plasmas adequate time to evolve to a state of thermal equilibrium.[8] For a system in which both the angular momentum and energy are conserved, the single-particle distribution function (Boltzmann distribution) takes the form[27–29]

$$f = n_0 \left(\frac{m}{2\pi k_B T} \right)^{3/2} \exp\left(-\frac{1}{k_B T} (H + \omega_r p_\theta) \right), \tag{4}$$

where

$$H = \frac{mv^2}{2} + q\phi(r,z), \tag{5}$$

$$p_\theta = m v_\theta r + \frac{qBr^2}{2c}. \tag{6}$$

Here H is the single particle Hamiltonian, p_θ is the canonical angular momentum of a single particle about the z axis, $\phi(r,z)$ is the electric potential, and k_B is Boltzmann's constant. The parameters n_0, ω_r, and T are determined by the total ion number, angular momentum, and energy of the system. We will see that ω_r is the plasma rotation frequency and, for a cold plasma, n_0 is the plasma density. If Eqs. (5) and (6) are substituted into Eq. (4), we find

$$f = n(r,z) \left(\frac{m}{2\pi k_B T} \right)^{3/2} \exp\left(-\frac{1}{2} m \frac{(\mathbf{v} + \omega_r r\hat{\theta})^2}{k_B T} \right), \tag{7}$$

where

$$n(r,z) = n_0 \exp\{ -[q\phi(r,z) + \tfrac{1}{2} m\omega_r(\Omega - \omega_r) r^2]/k_B T \}. \tag{8}$$

The density as a function of the coordinates r and z is given by $n(r,z)$ and $\Omega \equiv qB/(mc)$ is the cyclotron frequency. The velocity distribution in Eq. (7) describes a Maxwell–Boltzmann velocity distribution superimposed on a rigid-body rotation $\langle \mathbf{v} \rangle = -\omega_r r\hat{\theta}$. In particular, the plasma rotates without shear with frequency $-\omega_r$.

In the limit of low temperatures ($T \to 0$), if the plasma density in Eq. (8) is to remain finite in the plasma interior, the condition

$$q\phi(r,z) + \tfrac{1}{2}m\omega_r(\Omega-\omega_r)r^2 = 0 \tag{9}$$

must hold. The potential ϕ must be independent of z in the plasma interior. This is just the statement that there can be no force along a magnetic-field line in a zero temperature plasma. If the expression for $\phi(r,z)$ obtained from Eq. (9) is substituted into Poisson's equation, we see that the density is constant in the plasma interior and given by

$$n_0 = \frac{m\omega_r(\Omega-\omega_r)}{2\pi q^2}. \tag{10}$$

The plasma frequency is therefore related to the rotation frequency by

$$\omega_p^2 \equiv \frac{4\pi q^2 n_0}{m} = 2\omega_r(\Omega-\omega_r). \tag{11}$$

For finite temperatures, Eq. (8) and Poisson's equation imply that the ion density is constant up to the edge of the plasma and then drops off in a distance characterized by the Debye length[30]

$$\lambda_D \equiv \left(\frac{k_B T}{4\pi n_0 q^2}\right)^{1/2}. \tag{12}$$

The picture of a constant density plasma with sharp boundaries as $T \to 0$ is therefore valid for temperatures low enough that $\lambda_D \ll$ plasma dimensions.

The properties of rigid rotation and constant density result from the assumptions of thermal equilibrium and low temperature, and do not depend on a particular form of the trap potential. For the rest of this section, we assume a quadratic trap potential ϕ_T given by Eq. (1) with $V_0 = 0$. The total electrostatic potential ϕ is composed of three terms

$$\phi = \phi_T + \phi_I + \phi_{\text{ind}}. \tag{13}$$

Here ϕ_I is the potential due to the trapped ions and ϕ_{ind} is the potential due to the charges induced on the electrodes by the trapped ions. The potential ϕ_{ind} can be neglected when the trap dimensions are large compared to those of the plasma. This condition is achieved in many experiments and is assumed below. Solving for the ion potential using $\phi_I = \phi - \phi_T$ and Eq. (9), we find that inside the plasma

$$\phi_I = \frac{-m}{2q}[\omega_r(\Omega-\omega_r) - \omega_z^2/2]r^2 - \frac{m\omega_z^2 z^2}{2q}$$
$$= -\frac{m\omega_p^2}{6q}(ar^2 + bz^2), \tag{14}$$

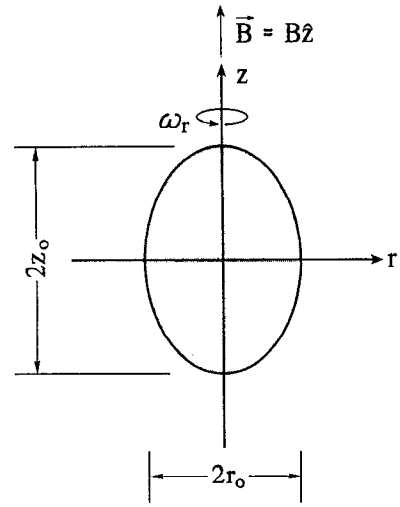

FIG. 2. Spheroidal shape of a Penning-trap plasma. This shape is obtained under the conditions of thermal equilibrium and $\lambda_D \ll$ (plasma dimensions) $\ll$ (trap dimensions).

where Eq. (14) defines a and b, and $2a+b=3$ as required by Poisson's equation. Here

$$\omega_z = \left(\frac{4qU_0}{m(r_T^2 + 2z_T^2)}\right)^{1/2} \tag{15}$$

is the frequency at which a single trapped particle (or the center of mass of a collection of particles) oscillates along the z axis. Equation (14) is just the potential in the interior of a uniformly charged spheroid. A spheroid is the shape obtained by rotating an ellipse about one of its principal axes. Let $2r_0$ and $2z_0$ denote the diameter and the axial extent of the plasma spheroid as shown in Fig. 2. The coefficients a and b are functions of the plasma aspect ratio $\alpha \equiv z_0/r_0$.[31–33] For example, when $\alpha = 1$ the plasma is spherical and $a = b = 1$. As $\alpha \to \infty$, the plasma becomes an infinitely long cylindrical column, and $a \to 3/2$ and $b \to 0$. As $\alpha \to 0$, the plasma becomes an infinitely thin disk, and $\alpha \to 0$ and $b \to 3$. The dependence of a and b on α and Eq. (14) show that the plasma frequency ω_p and the trap axial frequency ω_z are related by[31,32,34]

$$\frac{\omega_z^2}{\omega_p^2} = \frac{b(\alpha)}{3} = Q_1^0\left(\frac{\alpha}{(\alpha^2-1)^{1/2}}\right) \Big/ (\alpha^2-1), \tag{16}$$

where Q_l^m is the associated Legendre function of the second kind.

It is instructive to consider the plasma equilibrium as a function of rotation frequency ω_r for fixed trapping conditions (fixed ω_z, Ω, and number of ions N). Constant density equilibria exist when $\omega_z < \Omega/\sqrt{2}$ for rotation frequencies satisfying $\omega_m < \omega_r < \Omega - \omega_m$, where

$$\omega_m = \Omega/2 - (\Omega^2/4 - \omega_z^2/2)^{1/2} \tag{17}$$

is the single-ion magnetron frequency.[15] It is the $\mathbf{E}\times\mathbf{B}$ drift frequency at which a single trapped ion rotates about the trap symmetry axis. For ω_r slightly larger than ω_m, $\omega_z^2/\omega_p^2 \simeq 1$, and the plasma is shaped like a pancake (an

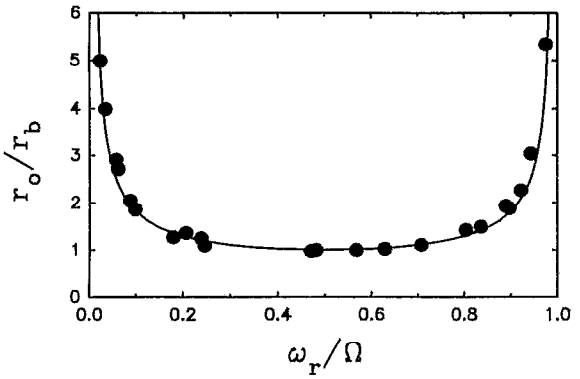

FIG. 3. Radius r_0 of a plasma of $\simeq 2000$ Be^+ ions as a function of rotation frequency ω_r. The radius is plotted in units of r_b, the plasma radius at the Brillouin limit, and the rotation frequency is plotted in units of the cyclotron frequency Ω. The solid line is a theoretical curve involving no adjustable parameters. The data were taken with $\Omega/2\pi = 1.4$ MHz and $\omega_z/\Omega = 0.151$ (from Ref. 34).

oblate spheroid). In the limit that $\omega_r \to \omega_m$, the plasma's aspect ratio $\alpha \to 0$, and the plasma's radius $r_0 \to \infty$. As ω_r increases, ω_z^2/ω_p^2 decreases and the plasma's aspect ratio α increases by decreasing r_0 and increasing z_0. At $\omega_r = \Omega/2$ the plasma attains its maximum aspect ratio (smallest r_0 and largest z_0) and maximum density $n_B = m\Omega^2/(8\pi q^2)$. The condition $\omega_r = \Omega/2$ is often called Brillouin flow.[1,2] In a frame of reference rotating with the plasma, the motion of an individual ion within the non-neutral plasma consists of circular gyrations (perturbed cyclotron orbits) at the frequency $\Omega - 2\omega_r$. At Brillouin flow, these gyrating orbits become free streaming (straight-line trajectories in the rotating frame), and the plasma behaves like an unmagnetized plasma. Therefore, at $\omega_r = \Omega/2$, a Penning-trap plasma behaves dynamically like a plasma confined in an RF (Paul) trap (if we can neglect the RF micromotion in the Paul trap—the forced small amplitude motion at ω_{rf}). As ω_r increases beyond $\Omega/2$, the plasma's aspect ratio α and density n_0 decrease. Because n_0 is an even function of ω_r about $\omega_r = \Omega/2$, the plasma's aspect ratio, radius, and axial extent are even functions of ω_r about $\omega_r = \Omega/2$. For example, as $\omega_r \to \Omega - \omega_m$, the plasma's aspect ratio α approaches 0, and the plasma's radius $r_0 \to \infty$. Figure 3 shows a graph of the radius of a plasma of $^9Be^+$ ions as a function of rotation frequency. Good agreement was obtained between the observed and predicted dependence of the plasma's radius on rotation frequency.

III. LASER COOLING AND STRONG COUPLING

The previous section on thermal equilibrium neglected any effects due to ion–ion correlations. Correlations become important at low temperatures. Equations (7) and (8) indicate that, except for a rigid rotation, ions in a Penning trap behave as if they are immersed in a uniform density background of opposite charge. Of course, this background charge density depends on ω_r. For a low temperature plasma, the ion charge density neutralizes the fictitious background charge density out to the plasma boundary. A single species of charge immersed in a uniform density background of opposite charge is a one-component plasma.[35] It follows that the static, thermodynamic properties of ions in a Penning trap are the same as those of a one-component plasma.[36] This is also true for ions in Paul traps if the micromotion is neglected. The thermodynamic properties of a one-component plasma are determined by the Coulomb-coupling parameter

$$\Gamma = \frac{q^2}{a_S k_B T}, \tag{18}$$

where a_S is the Wigner–Seitz radius given by $4\pi n_0 a_S^3/3 = 1$. Calculations[35,37] for the infinite one-component predict that for $\Gamma > 2$, the plasma should exhibit liquid-like behavior characterized by short range order, and at around $\Gamma = 170$ a liquid–solid phase transition to a body centered cubic (bcc) lattice should take place. With laser cooling, couplings of several hundred can be obtained with ions in traps.[13,38]

A. Doppler laser cooling

Laser light can be used to cool small samples of trapped ions and atoms to temperatures much less than 1 K. The simplest form of laser cooling and the one most commonly used for ions is called Doppler cooling.[32,39] It relies on the high spectral purity of lasers, the fact that atoms absorb light only at particular frequencies, and the frequency shift of the light (as viewed by the atom) due to the Doppler effect. Cooling results from the mechanical momentum imparted to the atoms when they scatter light; by suitable arrangement of a laser beam's frequency and direction, the atoms can be made to scatter light only when this scattering causes their momentum to be reduced. To illustrate, suppose an ion is constrained to move along the horizontal direction and is illuminated by a laser beam pointing along that direction. First, suppose the laser frequency is swept to measure the absorption spectrum of the ion near one of its optical transitions. If the ion is held stationary, the absorption would be particularly strong at a resonance frequency ω_0 with a narrow range γ outside which absorption drops rapidly (γ = Einstein A coefficient). For the resonance of interest in $^9Be^+$, $\omega_0/2\pi \simeq 10^{15}$ Hz and $\gamma/2\pi \simeq 20$ MHz.

Suppose we now release the ion and subject it to a laser beam coming from the left. Assume this laser has frequency ω_L, with $\omega_L < \omega_0$. If the ion moves to the left with velocity v, then in the ion's reference frame, the laser light appears to have a frequency approximately equal to $\omega_L(1+v/c)$ due to the first-order Doppler frequency shift. For particular values of v and ω_L, $\omega_L(1+v/c) \approx \omega_0$, and the ion absorbs and reemits photons at a high rate. On absorption, the photon's momentum is transferred to the ion and thereby reduces the ion's momentum by approximately h/λ (λ = the transition wavelength, h = Planck's constant). However, the photon reemission is spatially symmetric, so on the average, there is no net momentum imparted to the ion by reemission. Hence, on the average, the ion's momentum is reduced by h/λ for each scattering event.

If, instead, the atom moves to the right (along the laser beam direction), each scattering event increases the atom's momentum by $\hbar/\lambda$. However, the scattering rate is less for atoms moving to the right because the frequency of the radiation (in the atom's frame) is now $\omega_L(1-v/c) < \omega_L < \omega_0$, and the laser appears to be tuned away from the ion's resonance. This asymmetry in the scattering rate and in the accompanying transferred momentum of ions moving left or right, gives rise to cooling.

The randomness in the times of absorption and the randomness in the direction of photon reemission act like fluctuating impulses on the atom which counteract the cooling. These random impulses, which cause heating, reach a balance with the cooling when the effective temperature of the atoms reaches a minimum value, called the Doppler-cooling limit, equal to about $\hbar\gamma/2k_B$. For many ions, this temperature is around 1 mK or less. A temperature of 1 mK with densities greater than 10^7 cm^{-3} (see Sec. IV) gives couplings $\Gamma > 500$.

B. Shell structure

Ion trap experiments until now have laser-cooled small plasmas. Typical plasma dimensions are less than 20 interparticle spacings.[38] (In the quadrupole storage ring trap of Ref. 23, the plasmas were dimensionally large along the quadrupole circumference, but less than 8 interparticle spacings in the other directions.) It is not clear that such small systems will behave like infinite-volume one-component plasmas. A number of computer simulations[40–42] with less than a few thousand cold ions in a trap found something quite different than bcc order. The ions eventually froze into concentric, spheroidal shells rather than bcc planes. Each spheroidal shell consisted of a distorted two-dimensional hexagonal lattice. There was no well-defined liquid–solid phase transition; the freezing occurred over a broad range of couplings Γ. For example, oscillations in the density characteristic of shell structure was observed with $\Gamma < 10$. At $\Gamma \simeq 100$, very little diffusion occurred between shells, but very rapid diffusion was found within a shell.[42] For $\Gamma > 300$, the diffusion within a shell was also slow.[42]

Experimentally, shell structure has been observed with up to 20 000 laser-cooled Be^+ ions in a Penning trap.[38] The shells were observed by illuminating a thin cross section of the plasma with laser beams and imaging the laser-induced fluorescence onto a photon-counting imaging tube. Qualitative agreement was observed with the simulations, except that, in some cases, open-ended cylindrical shells were observed in the experiments. At present there is no convincing explanation for the open-ended cylindrical shells. One possibility is that shear in the plasma rotation might produce such a structure.

Strong coupling has also been attained with small ion clouds (typically less than 30 ions) in quadrupole RF traps.[43,44] For a recent review and complete list of references, see Ref. 45. Small "crystals" were observed by imaging the laser-induced fluorescence. Sudden changes in the configuration of the crystal were observed as the ratio of the trap's axial and radial restoring forces was varied. These structural phase transitions have been studied theoretically.[46–48]

How large must the ion plasmas be in order to observe infinite-volume behavior? Two different analytical methods[49,50] give similar predictions. The plasmas may have to be greater than 60 interparticle spacings along their smallest dimension in order to exhibit a bcc structure. For a spherical plasma, this means that the number of trapped ions must be greater than 10^6. A Penning trap designed for trapping and laser cooling a few million Be^+ ions is being tested at the National Institute of Standards and Technology (NIST).[51]

C. Linear RF trap results

Recently, linear RF traps have been used to create one-dimensional and other types of strongly coupled structures. Elongated, crystallized ion structures have been observed in a linear Paul trap by the group at Garching.[23,45] They used a configuration in which the trap electrodes were bent into rings and closed on themselves to form a torus. They observed various structures ranging from a single string on the axis of the trap to more complex shapes like multiple layers of intertwined helices. These structures agree with simulations of crystallized structures expected for particles in high-energy storage rings.[40,52,53] If these structures can be formed in storage rings, high-energy beams with significantly increased brightness could be used in collision experiments.

In experiments at NIST, similar structures were observed, but in a linear trap with a much less elongated geometry using four parallel straight rods.[22] In a demonstration experiment,[54] the NIST researchers were able to observe the interference scattering from two ions localized in the trap. This can be viewed as a kind of Bragg scattering experiment in the limit of the smallest number (two) of particles. The NIST researchers plan to investigate the use of a single strand of ions confined in a linear trap for an atomic clock.[4] The main advantage of this configuration is that the kinetic energy of the micromotion of the ions and the accompanying time-dilation frequency shift can be made very small.

Strings of ions may also be viewed as one-dimensional (1-D) plasmas. These plasmas would be expected to show interesting differences when compared to two- and three-dimensional plasmas. For example, the strong anisotropy of the 1-D plasma is expected to strongly reduce the rate at which ion–ion interactions transfer kinetic energy between degrees of freedom associated with motions parallel and perpendicular to the trap axis.[55,56]

The crystallized ion structures observed in elongated linear Paul traps are essentially the same as those which are expected for ions in an elongated Penning trap. The intertwined helices can be thought of as lying on shells; these shells correspond to the shells observed in Penning traps. In the Paul trap, the ions do not (necessarily) rotate around the trap axis; this greatly facilitates the observation of crystallized structures, since they can be observed by direct imaging. On the other hand, micromotion causes

heating of ions in Paul traps. This heating becomes stronger as the diameter of the plasmas increase. Therefore large diameter structures appear to be more easily studied in Penning traps, where this source of heating is absent.

D. Sub-Doppler laser cooling

In 1988, an important experiment[57] showed that laser-cooling temperatures lower than the Doppler-cooling limit could be obtained for atomic transitions involving more than two levels.[58] One way this works is as follows: When an atom or ion is illuminated by laser radiation, the atomic electrons, attached to the atomic core, experience a ponderomotive force in the fields of the laser. If the laser frequency is turned above a particular transition, this force is entirely analogous to the ponderomotive force responsible for trapping ions in a Paul trap, and the atom experiences an "optical potential" which forces it toward regions of weaker field amplitude. (In general, the strength and sign of the optical potential depends on the internal state of the atom and frequency of the laser.) When an atom moves from a region of weaker optical potential to stronger potential, it loses kinetic energy. If, after running up an optical potential hill, the atom changes (or is optically pumped) to a third internal state which does not experience an optical potential, its kinetic energy is less than its original value. Later, it can be optically pumped back to its original state (without changing its kinetic energy), where the process starts over again. If, instead, the atom runs down a potential hill and then is pumped to the third state, it gains kinetic energy. However, it is possible to find situations where the atoms are preferentially pumped to the third state after running up a potential hill and net cooling occurs. This particular form of cooling is called "Sisyphus" cooling after the person in Greek mythology who was condemned to repeatedly carry a rock to the top of a hill only to have it roll down each time.

In sub-Doppler cooling schemes,[58] the limiting kinetic energy for a free atom is approximately equal to the kinetic energy it would receive if it was originally at rest and recoiled upon the emission of a single photon. This corresponds to a temperature of about 1 μK. Similar temperatures could be expected for trapped ions. In this regime $k_B T \ll \hbar\omega_p$, so the plasma modes must be treated quantum mechanically.

IV. LASER BEAM TORQUES

A. Control of the plasma rotation frequency

In most Penning-trap experiments, the rotation frequency ω_r is much less than $\Omega/2$, corresponding to low densities and strongly magnetized plasmas. In laser-cooled Penning-trap plasmas, the lasers can also be used to provide a torque to increase the ion density and access all possible thermal equilibria, including Brillouin flow. This is done by directing a laser beam to the side of the rotating plasma that recedes from the laser beam, as shown in Fig. 4. In Fig. 4, the laser applies a torque whose sign is negative; this will decrease the angular momentum P_θ about the trap's z axis. If $\omega_r \ll \Omega$, Eq. (3) shows that the plasma radius will decrease; the plasma density and rotation frequency increase accordingly. In general, the plasma radius will decrease and the ion density increase until the torque due to the laser beam is offset by some other torque, for example, due to asymmetries in the trap construction. In this manner the slow radial expansion of a Penning trap plasma which normally occurs can be stopped, and a steady state distribution can be obtained.

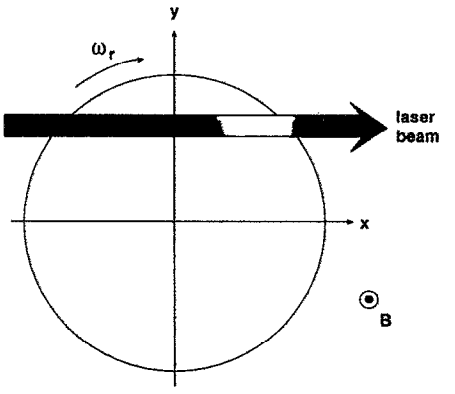

FIG. 4. Plasma cross section showing the position of the laser beam for applying a torque which decreases the plasma canonical angular momentum and increases the plasma rotation frequency. The magnetic field is out of the page and positively charged trapped ions are assumed. In Refs. 34 and 59, laser torques were used to achieve all possible thermal equilibria, including Brillouin flow.

In experiments[34,59] with laser-cooled Be^+ ions, laser torques were used to increase the plasma rotation frequency and obtain all possible thermal equilibria. Typically one laser beam was used to cool the plasma, and one beam was directed near the radial edge of the plasma to apply a strong torque to the plasma. The applied torque was changed by varying the frequency of the torque beam. Initially with $\omega_r \ll \Omega$, the frequency of the torque laser beam was tuned below the cooling transition frequency which produced very little ion fluorescence and torque. As the torque laser frequency was increased above the cooling transition frequency, the torque laser became resonant with the Doppler shifted ions in the beam path. This produced ion fluorescence and a torque on the plasma which increased the plasma rotation frequency. The plasma rotation frequency could be increased smoothly through Brillouin flow to frequencies slightly less than the cyclotron frequency, except for a small range of rotation frequencies where the plasma acquired a diffuse boundary and low ion fluorescence characteristic of a hot plasma.[59] An explanation of the apparent heating is given in the next section. The rotation frequency was measured from the Doppler-generated sidebands produced by the rotation on the electron spin flip transition in the ground state of Be^+.[59] With laser-cooled Be^+ ions at $B=0.8$ T, the ion density ranged from 10^7 cm^{-3} at low rotation frequency to 2×10^8 cm^{-3} at the Brillouin limit. At 6 T, a density of about 1×10^{10} cm^{-3} was obtained at the Brillouin limit.

B. Plasma rotation and atomic clock frequency shifts

In an atomic clock, the relative frequency imprecision due to intrinsic measurement noise scales as $N^{-1/2}$ (Ref. 25) where N is the number of ions. Therefore, to reduce the imprecision, we desire to make N as large as possible. However, as we increase the number of ions in a Penning-trap plasma, the size of the plasma increases and the velocity in the rotational motion also increases. One of the largest systematic frequency shifts in an ion trap frequency standard is the second-order Doppler shift (or time-dilation shift) due to the small but nonzero kinetic energy of the ions. For plasmas that are laser cooled, the kinetic energy in the rotational motion dominates over the thermal kinetic energy of the plasma except for highly prolate plasmas that are nearly confined to the trap axis.

The time-dilation frequency shift due to the plasma rotation is given by $\Delta\nu_{D2}/\nu_0 \simeq -\omega_r^2\langle r^2\rangle/2c^2$, where $\langle r^2\rangle$ is the mean square radius of the plasma and the shift is expressed as a fraction of the clock transition frequency ν_0. This frequency shift may be difficult to measure precisely, which would limit the accuracy of the clock. The frequency shift may also fluctuate due to fluctuations in plasma parameters such as the rotation frequency or plasma radius. This will cause the clock's frequency to fluctuate, and reduce the stability at long measurement times.

Near the Brillouin limit, where the radius of the plasma goes through a minimum, $\Delta\nu_{D2}$ increases as ω_r^2. Here the time-dilation shift is large and sensitive to fluctuations in ω_r. On the other hand, for very low rotation frequencies $\omega_r \to \omega_m$, the plasma radius rapidly increases with small decreases in ω_r (see Fig. 3). Here the time-dilation shift is also large and sensitively depends on ω_r. It follows that, for a given ω_z and Ω, there is a rotation frequency ω_r where the time-dilation shift is a minimum and depends only on fluctuations in the rotation frequency to second order. Improved frequency standard performance can be obtained by stabilizing ω_r to this optimum rotation frequency.

V. ELECTROSTATIC MODES

Much progress has been made recently in understanding the collective oscillations of small, cold, non-neutral plasmas trapped in Penning traps. In several recent experiments, both magnetized plasma[34,59–61] and upper hybrid[34] oscillations have been excited and studied. The measured frequencies agree with a recent cold fluid theory for the normal modes of a magnetized plasma spheroid,[62] although in one experiment[60] noticeable frequency shifts were induced by the effects of finite temperature and trap anharmonicity. These effects are a subject of current theoretical work,[60,63] and we will briefly describe one approach in this section.

Excitation and detection of plasma modes may have several applications. Since the mode frequencies depend on the density, rotation frequency, temperature, and shape of the plasma, a measurement of mode frequencies may provide a diagnostic for these important plasma parameters. This technique may be particularly valuable as a nondestructive diagnostic for experiments where laser fluorescence techniques are inapplicable, such as those involving electron, positron,[64] or antiproton[65] plasmas. Other techniques for obtaining information about these plasmas involve ejecting the plasma from the trap, and are thus destructive.

Collective modes can also play an important role in plasma confinement.[66] Field errors in the trapping potential can excite plasma modes and thereby enhance loss of the plasma. Excitation of the plasma modes can therefore set a practical limit on the density and number of particles stored in a Penning trap. Resonances of plasma modes with static field errors have already been observed to heat the plasma and limit the density in Penning-trap experiments.[34,59]

Measurement of the electrostatic modes of a Penning-trap plasma can also be a useful tool for studying the dynamics of non-neutral plasmas under various conditions. Such studies have already provided important insights into plasma behavior in long cylindrical traps in which the confinement potentials are not harmonic.[10] The effect of finite length on the linear modes of such a plasma has previously been considered only through approximations such as perturbation theory applied to an approximate finite-length equilibrium.[67] On the other hand, an analytic form for all the electrostatic cold fluid eigenmodes and eigenfrequencies has recently been found for small, cold spheroidal plasmas in a Penning trap.[62] This is the only realistic finite-length geometry for which exact fluid mode eigenfrequencies and eigenfunctions have been calculated. A Penning trap with nearly pure quadrupole electrostatic potential may therefore be a useful geometry for non-neutral plasma studies when a detailed understanding of eigenmode structure and frequency is needed. For example, for cryogenic plasmas a measurement of the shifts of the mode frequencies from the predictions of cold fluid theory can be related to the bulk and shear moduli of the plasma.[68] A measurement of the damping of the modes may provide information on the plasma viscosity. Such measurements could be performed with a strongly correlated plasma over a range of magnetic field strengths where very little information is presently available.

A. Theoretical developments

We first briefly describe recent theoretical developments in the fluid theory of normal modes in trapped non-neutral plasmas. Section II showed that a non-neutral plasma in thermal equilibrium in a harmonic trap at zero temperature is a uniform density spheroidal plasma rotating at frequency ω_r. In cold fluid theory the linear electrostatic normal modes of this plasma are described by Maxwell's equation for the perturbed potential $\psi(\mathbf{x},t)$

$$\nabla\cdot\boldsymbol{\epsilon}(\mathbf{x})\cdot\nabla\psi=0, \tag{19}$$

where $\boldsymbol{\epsilon}(\mathbf{x})$ is the dielectric tensor for the magnetized plasma spheroid

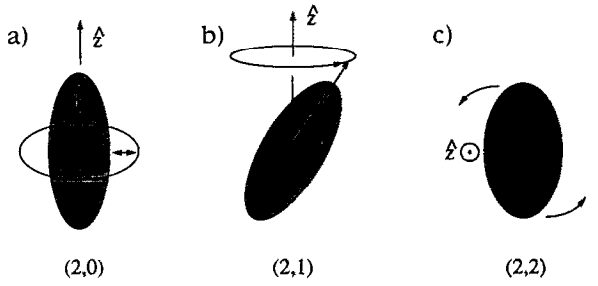

FIG. 5. Schematic picture of the three $l=2$ normal modes of oscillation. (a) The (2,0) mode is an oscillation of the length and radius of a spheroid whose axis of symmetry is oriented along the z direction. (b) The (2,1) mode is a slight tilt of the plasma with respect to z; the tilted plasma then precesses around the z axis. (c) In the (2,2) mode, the plasma is slightly distorted into a triaxial ellipsoid with a principal axis along the z direction. The ellipsoid then rotates around the z axis (from Ref. 63).

$$\epsilon=\begin{bmatrix}\epsilon_1 & -i\epsilon_2 & 0\\ i\epsilon_2 & \epsilon_1 & 0\\ 0 & 0 & \epsilon_3\end{bmatrix},$$

with $\epsilon_1=1-\omega_p^2/(\omega^2-\Omega_v^2)$, $\epsilon_2=\Omega_v\omega_p^2/[\omega(\omega^2-\Omega_v^2)]$, and $\epsilon_3=1-\omega_p^2/\omega^2$. Here ω is the mode frequency as seen in a frame rotating with the plasma and $\Omega_v=\Omega-2\omega_r$ is the vortex frequency, which is the cyclotron frequency in the rotating frame. The boundary conditions we consider are $\psi=0$ at $|\mathbf{x}|\to\infty$ (image charges are neglected).

Analytic solutions of Eq. (19) are generally available in only a few standard geometries for which a separable solution can be found, and a spheroidal Penning-trap plasma is not a standard geometry. However, Dubin[62] showed that Eq. (19) is separable for a spheroidal Penning-trap plasma in an unusual set of frequency dependent coordinates. The normal modes can be thought of as spheroidal harmonics. That is, outside the plasma the mode potential takes the form

$$\psi^{\text{out}}=Ae^{-i\omega t+im\phi}Q_l^m(\xi_1/d)P_l^m(\xi_2), \tag{20}$$

where Q_l^m and P_l^m are Legendre functions, (ξ_1,ξ_2,ϕ) are spheroidal coordinates (Ref. 69), $d\equiv\sqrt{z_0^2-r_0^2}$ is half the distance between the foci of the plasma spheroid, and l and m are mode numbers determining the order of the spheroidal harmonic. For a spherical plasma, $d\to 0$, (ξ_1,ξ_2,ϕ) approach spherical coordinates $(r,\cos\theta,\phi)$, and ψ^{out} approaches the usual form for a spherical multipole moment, $\psi^{\text{out}}\sim e^{-i\omega t+im\phi}r^{l-1}P_l^m(\cos\theta)$. Inside the cloud, the potential variation depends on mode frequency; details may be found in Refs. 34 and 62.

B. Experimental measurements

Some of the $l=2$ modes have been measured in the NIST laser-cooled ion experiments. These are quadrupole excitations, which in general correspond to deformations of the spheroid into a triaxial ellipsoid (an ellipsoid in which the three principal axes differ in length) with a time-dependent shape and/or orientation.[63] The form of these $l=2$ modes are shown in Fig. 5. For $l=2$ and $m=0$, the mode corresponds to axisymmetric radial and axial compressions of the spheroid. For large vortex frequency $|\Omega_v|$ the radial compressions are upper hybrid oscillations near the cyclotron frequency, while the axial compressions are magnetized plasma oscillations at some fraction of the plasma frequency. A comparison between theory[34,62] and experiment[34,59] for the dependence of these mode frequencies on the plasma shape (or rotation frequency) is shown in Fig. 6 for the laser-cooled ion plasmas. In these experiments, the mode is excited by applying a sinusoidal potential between the ring and endcap electrodes. The modes were detected by a change in the ion fluorescence when the applied frequency was resonant with the mode frequency. As Fig. 6 shows, excitation of the (2,0) modes may be a useful way to determine the plasma rotation frequency, or equivalently the plasma shape, for a broad range of ω_r/Ω values.

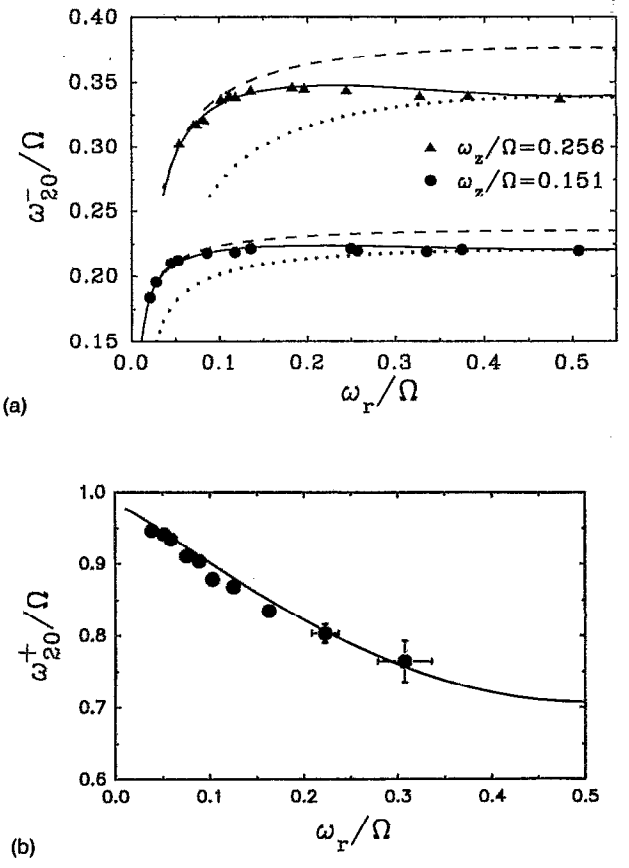

FIG. 6. (a) Plasma mode frequency ω_{20}^- as a function of the rotation frequency ω_r. The circles and triangles give the experimental data. The solid line gives the cold-fluid model predictions. The dashed and dotted lines give the high- and low-magnetic-field calculations for ω_{20}^-, respectively. (b) Upper hybrid mode frequency ω_{20}^+ as a function of the rotation frequency ω_r for $\omega_z/\Omega=0.151$. The circles give the experimental data. The solid line gives the cold-fluid model predictions. All frequencies are expressed in units of the cyclotron frequency Ω (from Ref. 34).

Recently, an experiment at NIST used plasma modes to determine the aspect ratio of pure electron plasmas in a cryogenic (4 K) Penning trap.[61] The modes were detected through image currents induced in one of the endcap electrodes. Experimentally, modes with frequencies near the

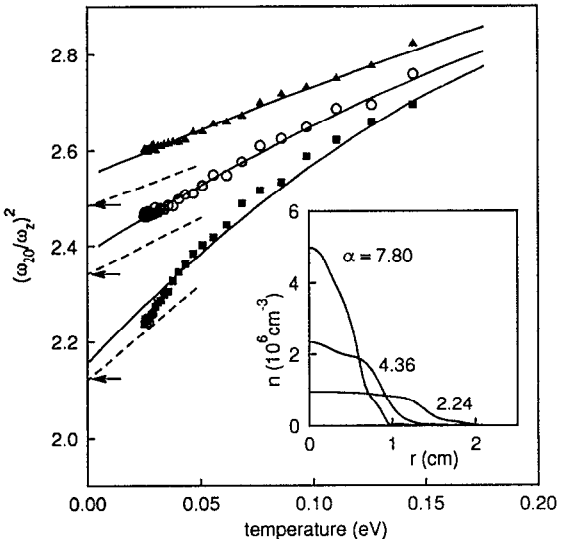

FIG. 7. Temperature dependence of the quadrupole mode frequency for electron plasmas with different shapes: (■), $\alpha_0=2.24$, $2z_0=6.20$ cm; (○), $\alpha_0=4.38$, $2z_0=7.52$ cm; and (▲), $\alpha_0=7.80$, $2z_0=8.32$ cm. Solid lines are the results of numerical simulations of the plasmas (Ref. 60). Arrows on the vertical axis show the cold fluid theory predictions; dashed lines are from Eq. (29). The inset shows the radial density profiles of these plasmas (from Ref. 60).

single-particle axial frequency ω_z could be detected. Immediately after a plasma of electrons was loaded into the trap, only the center-of-mass mode was observed. However, after a period of time that depended on the magnetic field, other modes were observed. The evolution of the mode frequencies was followed as a function of time. The detected modes were identified within the framework of Dubin's cold fluid theory[62] as drumhead modes of a two-dimensional disk. With some plasmas up to eight modes were identified which were used to provide seven different estimates of the plasma aspect ratio. The discrepancy between the different estimates was less than 20%. The drumhead modes were detected when the plasma aspect ratio α was about 0.02 or smaller. The decrease in α as a function of time could then be followed until $\alpha \simeq 0.002$. In these experiments the number of electrons, determined from the center-of-mass mode signal, was between 20 000 and 100 000. Measurement of the plasma modes was the only known method for determining the plasma shape.

C. Effects beyond cold fluid theory

The low-frequency (2,0) quadrupole mode has also been measured in pure electron plasmas which are cooled by collisions with a buffer gas to near room temperature.[60] Here the modes were also detected through the image charges they induced on the surrounding electrode structure. In these experiments the Debye length λ_D was not negligible compared to the plasma size, the plasma was not in thermal equilibrium, and the plasma was not necessarily small compared to the electrode diameters. Nevertheless, the cold fluid theory works fairly well as a starting point in describing the (2,0) frequency (see Fig. 7). However, in order to explain the observed increase in mode frequency as temperature increases, it is necessary to go beyond the cold fluid limit. For relatively cold plasmas where λ_D is small compared to the plasma dimensions, the frequency shift can be accounted for by keeping pressure terms in the fluid equations.

We illustrate the effects of pressure in fluid theory by considering the (2,0) plasma oscillations in the limit that the magnetic field is very large. In this case the plasma oscillation occurs only in the z direction and the equilibrium and linear dynamics are described by

$$mn\frac{d^2\delta z}{dt^2}=-qn\frac{\partial\phi}{\partial z}-\frac{\partial p}{\partial z}, \tag{21}$$

where p is the pressure, $\delta z(\mathbf{x},t)$ is the z displacement of a fluid element from its equilibrium position $\mathbf{x}$, n is the density, and ϕ the total electrostatic potential. In equilibrium the plasma satisfies

$$-qn_0\frac{\partial\phi_0}{\partial z}=\frac{\partial p_0}{\partial z}, \tag{22}$$

where $p_0=n_0k_BT$ is the equilibrium pressure, we assume T is constant, and n_0 is the equilibrium density. We note that for finite T, Eq. (22) implies that n_0 is no longer perfectly uniform within the plasma; now the plasma has a smooth edge with a width on the order of λ_D.

Perturbations away from equilibrium are described by $p=p_0+\delta p$, $\phi=\phi_0+\psi$, and $n=n_0+\delta n$. The perturbed density δn is related to the fluid displacement δz through the linearized continuity equation

$$\delta n=-\frac{\partial}{\partial z}(n_0\delta z). \tag{23a}$$

The perturbed pressure δp is related to the fluid displacement by

$$\delta p=-\delta z\frac{\partial p_0}{\partial z}+\gamma p_0\frac{\partial\delta z}{\partial z}, \tag{23b}$$

where the first term describes the pressure change at a fixed point due to convection, the second term is the pressure change due to compression, and γ is the ratio of specific heats. We assume an adiabatic law for these 1-D expansions and compressions, so $\gamma=3$. Equations (22) and (23) can then be used in Eq. (21) to yield an equation for the fluid displacement δz induced by the perturbing field

$$\omega^2\delta z=\frac{q}{m}\left(\frac{\partial\psi}{\partial z}+\delta z\frac{\partial^2\phi_0}{\partial z^2}\right)-\frac{\gamma k_BT}{mn_0}\frac{\partial}{\partial z}\left(n_0\frac{\partial\delta z}{\partial z}\right), \tag{24}$$

where ω is the mode frequency.

Equations (23a) and (24), and Poisson's equation $\nabla^2\psi=-4\pi q\delta n$ constitute a closed set of partial differential equations for δn, ψ, and δz which can be solved as a straightforward (though tedious) numerical eigenvalue problem for the mode frequency. However, rather than resorting to numerical solutions we instead apply a simple ansatz to obtain an analytic expression for the mode frequency ω which approximately describes the effect of finite temperature. We assume that the plasma remains a uni-

form spheroid,[63] although this is rigorously correct only when $T \to 0$ and anharmonic and image charge effects are negligible. The equilibrium shape of the spheroid is then determined by taking a moment of Eq. (22). Multiplying Eq. (22) by z and integrating, we obtain

$$\int q n_0 z \frac{\partial \phi_0}{\partial z} d^3x = N k_B T. \tag{25}$$

Since $\phi_0 = \phi_{ext} + \phi_I$ where $\phi_{ext} = \phi_T + \phi_{ind}$, Eq. (25) determines the aspect ratio α in terms of r_0, T, N, and the external potential. Anharmonic effects in ϕ_{ext} and image charges could be kept, but for now we neglect such effects and use the harmonic form for $\phi_{ext} = \phi_T$ and ϕ_I, Eqs. (1) and (14). The integral over the spheroid in Eq. (25) can be performed, yielding an expression for the equilibrium plasma shape α that includes the effect of temperature

$$1 - \frac{a_0^3}{r_0^3} \frac{b(\alpha)}{\alpha} = \frac{5 k_B T}{m \omega_z^2 r_0^2 \alpha^2}, \tag{26}$$

where $a_0 = (Nq^2/m\omega_z^2)^{1/3}$ is a length scale on the order of the plasma size. Equation (26) implies, as T increases, that the plasma increases in length, in agreement with intuition. (Throughout this analysis the spheroid radius r_0 is assumed to be fixed because the experiments are carried out rapidly compared to radial transport times.)

Turning to the perturbations around this equilibrium, our ansatz of purely spheroidal perturbations implies that plasma motion can be described as a change in the length of the spheroid by a small amount $\epsilon(t) z_0$. The perturbed electric field is then determined by a Taylor expansion of Eq. (14). We obtain

$$\frac{\partial \psi^{in}}{\partial z} = -\epsilon \frac{m}{q} \omega_z^2 \frac{a_0^3}{r_0^3} \alpha \frac{\partial}{\partial \alpha} \left(\frac{b}{\alpha} \right) z. \tag{27}$$

Furthermore, our ansatz implies $\delta z = \epsilon z$ in order to satisfy the assumption of uniform density. Substitution of these relations into Eq. (24), multiplication by $n_0 z$ and integration over the spheroid then yields the following approximate expression for the (2,0) mode frequency:

$$\omega^2 = \omega_z^2 \left(1 - \frac{a_0^3}{r_0^3} \frac{\partial b}{\partial \alpha} \right) + \frac{5 \gamma k_B T}{m z_0^2}. \tag{28}$$

The last term in Eq. (28) is a frequency increase similar to that expected in the Bohm–Gross dispersion relation $\omega^2 = \omega_p^2 + \gamma k_B T k_z^2 / m$, where the parallel wave number k_z is of order $1/z_0$. However, the first terms in Eq. (28) also depend on T through the change of the equilibrium shape α as T increases, given by Eq. (26). Assuming that the temperature effect is small, we keep temperature corrections to α only to lowest order in T, in which case Eq. (28) becomes[60]

$$\omega^2 = \omega_0^2(\alpha_0) + \frac{k_B T}{m (2 z_0)^2} f(\alpha_0), \tag{29}$$

where α_0 is the plasma shape at $T = 0$ [the solution of Eq. (26) at $T = 0$], $\omega_0^2(\alpha_0)$ is the (2,0) frequency at $T = 0$, and

$$f(\alpha_0) \equiv 20 \left(\gamma - \frac{\alpha_0^2}{b(\alpha_0) \omega_0^2(\alpha_0)} \frac{\partial^2 b}{\partial \alpha_0^2} \right).$$

For the experiments at NIST, the temperature effects are negligibly small, but in the experiments at UCSD these effects are not negligible. In Fig. 7 we compare the theoretical frequency of Eq. (29) with the experimental measurement.[60] There is fair agreement, even though the radial density profile is not very close to that of a uniform spheroid, and we have neglected image charges and anharmonic effects in our analysis. Indeed, particle-in-cell simulations of the modes[60] which include these effects observe very good agreement with the experiments (see Fig. 7), so there is hope that including these effects in the analytic model may also improve agreement with the experiments.

D. Resonant interactions with static field errors

Resonant interactions between normal modes and an external static error in the trap fields have also been observed.[34,59] Such interactions may heat the plasma and limit ion confinement. In the experiments, a range of plasma rotation frequencies was observed where the plasma acquired a diffuse boundary and a low level of fluorescence characteristic of a hot plasma. The range over which this apparent heating occurred depended sensitively on the angle θ_0 between the trap's symmetry axis and the magnetic field direction. For $\theta_0 > 0.1°$ the plasma rotation frequency could not be increased beyond the point where heating first occurred. The heating appeared to get stronger with an increase in the number of ions. Furthermore, θ_0 could be adjusted to less than 0.01° by searching for an alignment which gave no apparent heating (assuming that the trap is aligned when the heating is minimized).

This heating resonance has been identified as an excitation of an $l = 2$ and $m = 1$ plasma mode by the asymmetry associated with the misalignment of trap and magnetic axes. The (2,1) mode consists of a tilt of the plasma spheroid with respect to the magnetic axis. The spheroid then precesses around the axis at one of three possible rates for

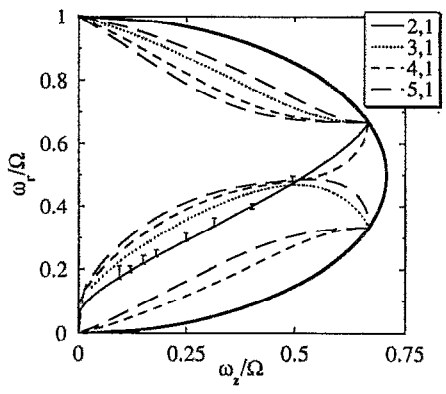

FIG. 8. Values of ω_r/Ω and ω_z/Ω for which different $m = 1$ modes are predicted to be zero frequency in the laboratory frame. Points with error bars are experimental measurements of the location of the heating resonance. The thick curve is the confinement boundary given by Eq. (17), beyond which there is no thermal equilibrium (from Ref. 34).

given plasma rotation frequency and shape [see Fig. 5(b)]. For certain plasma parameters this mode can be zero frequency in the laboratory frame; that is, the precession can be equal in magnitude and opposite in direction to the rotation frequency, so that the plasma shape appears to be a stationary tilted spheroid in the laboratory frame (within this shape the plasma continues to circulate). The mode can then resonantly interact with a static field error.

Figure 8 shows the measured rotation frequencies ω_r where heating occurred for different trap axial frequencies ω_z, when the trap was misaligned by $\theta_0 \simeq 0.02°$. Also shown (solid line) is the rotation frequency at which the (2,1) mode has zero frequency in the laboratory frame of reference, calculated from the cold fluid dispersion relation.[34,59,62] There is excellent agreement between the predicted and measured resonant rotation frequencies. Shown for comparison in this figure are predictions for when other $m=1$ modes reach zero frequency in the laboratory frame.[34] These other modes may also cause heating resonances. In experiments on larger plasmas several heating resonances have been observed, although as yet they have not been identified.

ACKNOWLEDGMENTS

We gratefully acknowledge the support of the Office of Naval Research. The research of DHED is also supported by the National Science Foundation. We also acknowledge the contribution of many co-workers during the past 10 years, including Jim Bergquist, Larry Brewer, Sarah Gilbert, Dan Heinzen, Wayne Itano, Dan Larson, Fred Moore, Tom O'Neil, John Prestage, Mark Raizen, Joseph Tan, and Carl Weimer. We thank Amy Barton, Joseph Tan, and Matt Young for their suggestions and careful reading of the manuscript.

[1]R. C. Davidson, *Physics of Non-Neutral Plasmas* (Addison–Wesley, Redwood City, CA, 1990).
[2]*Non-Neutral Plasma Physics*, edited by C. W. Roberson and C. F. Driscoll (American Institute of Physics, New York, 1988).
[3]W. M. Itano and N. F. Ramsey, Sci. Am. **269**, 56 (1993).
[4]J. J. Bollinger, D. J. Heinzen, W. M. Itano, S. L. Gilbert, and D. J. Wineland, IEEE Trans. Instrum. Meas. **40**, 126 (1991); D. J. Wineland, J. C. Bergquist, J. J. Bollinger, W. M. Itano, D. J. Heinzen, S. L. Gilbert, C. H. Manney, and M. G. Raizen, IEEE Trans. Ultrasonics, Ferroelectrics, Frequency Control **37**, 515 (1990).
[5]L. S. Cutler, R. P. Giffard, P. J. Wheeler, and G. M. R. Winkler, in *Proceedings of the 41st Annual Frequency Symposium, 1987*, p. 12 (see National Informational Service document no. AD-A216858. Copies may be ordered from the National Technical Information Service, Springfield, VA 22161).
[6]J. D. Prestage, G. J. Dick, and L. Malecki, IEEE Trans. Instrum. Meas. **40**, 132 (1991).
[7]J. J. Bollinger, J. D. Prestage, W. M. Itano, and D. J. Wineland, Phys. Rev. Lett. **54**, 1000 (1985).
[8]C. F. Driscoll, J. H. Malmberg, and K. S. Fine, Phys. Rev. Lett. **60**, 1290 (1988).
[9]T. M. O'Neil, Phys. Fluids **23**, 725 (1980).
[10]J. H. Malmberg, C. F. Driscoll, B. Beck, D. L. Eggleston, J. Fajans, K. Fine, X.-P. Huang, and A. W. Hyatt, in Ref. 2, pp. 28–71.
[11]D. J. Wineland and H. G. Dehmelt, J. Appl. Phys. **46**, 919 (1975).
[12]J. Tan and G. Gabrielse, Phys. Rev. A **48**, 3105 (1993).
[13]J. J. Bollinger and D. J. Wineland, Phys. Rev. Lett. **53**, 348 (1984); W. M. Itano, L. R. Brewer, D. J. Larson, and D. J. Wineland, Phys. Rev. A **38**, 5698 (1988).
[14]F. M. Penning, Physica **3**, 873 (1936).
[15]H. G. Dehmelt, Adv. At. Mol. Phys. **3**, 53 (1967); **5**, 109 (1969).
[16]D. J. Wineland, W. M. Itano, and R. S. Van Dyck, Jr., Adv. At. Mol. Phys. **19**, 135 (1983).
[17]R. C. Thompson, Adv. At. Mol. Opt. Phys. **31**, 63 (1993).
[18]W. Paul and H. Steinwedel, Z. Naturforsch. A **8**, 448 (1953).
[19]E. Fisher, Z. Phys. **156**, 1 (1959).
[20]D. J. Bate, K. Dholakia, R. C. Thompson, and D. C. Wilson, J. Mod. Opt. **39**, 305 (1992).
[21]J. H. Malmberg and J. S. deGrassie, Phys. Rev. Lett. **35**, 577 (1975).
[22]M. G. Raizen, J. M. Gilligan, J. C. Bergquist, W. M. Itano, and D. J. Wineland, Phys. Rev. A **45**, 6493 (1992).
[23]G. Birkl, S. Kassner, and H. Walther, Nature **357**, 310 (1992).
[24]H. G. Dehmelt, Bull. Am. Phys. Soc. **20**, 60 (1975).
[25]W. M. Itano, J. C. Bergquist, J. J. Bollinger, J. M. Gilligan, D. J. Heinzen, F. L. Moore, M. G. Raizen, and D. J. Wineland, Phys. Rev. A **47**, 3554 (1993).
[26]T. M. O'Neil, Phys. Fluids **23**, 2216 (1980).
[27]In Ref. 1, pp. 52–59, 110–115.
[28]T. M. O'Neil, in Ref. 2, pp. 6–10.
[29]L. D. Landau and E. M. Lifshitz, *Statistical Physics* (Addison–Wesley, Reading, MA, 1974), p. 11.
[30]S. A. Prasad and T. M. O'Neil, Phys. Fluids **22**, 278 (1979).
[31]L. R. Brewer, J. D. Prestage, J. J. Bollinger, W. M. Itano, D. J. Larson, and D. J. Wineland, Phys. Rev. A **38**, 859 (1988).
[32]D. J. Wineland, J. J. Bollinger, W. M. Itano, and J. D. Prestage, J. Opt. Soc. Am. B **2**, 1721 (1985).
[33]J. B. Jeffries, S. E. Barlow, and G. H. Dunn, Int. J. Mass Spectrom. Ion Processes **54**, 169 (1983).
[34]J. J. Bollinger, D. J. Heinzen, F. L. Moore, W. M. Itano, D. J. Wineland, and D. H. E. Dubin, Phys. Rev. A **48**, 525 (1993).
[35]S Ichimaru, H. Iyetomi, and S. Tanaka, Phys. Rep. **149**, 91 (1987).
[36]J. H. Malmberg and T. M. O'Neil, Phys. Rev. Lett. **39**, 1333 (1977).
[37]E. Pollack and J. Hansen, Phys. Rev. A **8**, 3110 (1973); W. L. Slaterly, G. D. Doolen, and H. E. DeWitt, *ibid.* **21**, 2087 (1980); **26**, 2255 (1982); S. Ogata and S. Ichimaru, *ibid.* **36**, 5451 (1987); D. H. E. Dubin, *ibid.* **42**, 4972 (1990).
[38]S. L. Gilbert, J. J. Bollinger, and D. J. Wineland, Phys. Rev. Lett. **60**, 2022 (1988).
[39]See, for example, D. J. Wineland and W. M. Itano, Phys. Today **40**, 34 (1987).
[40]A. Rahman and J. P. Shiffer, Phys. Rev. Lett. **57**, 1133 (1986).
[41]H. Totsuji, in *Strongly Coupled Plasma Physics*, edited by F. J. Rogers and H. E. DeWitt (Plenum, New York, 1987), p. 19.
[42]D. H. E. Dubin and T. M. O'Neil, Phys. Rev. Lett. **60**, 511 (1988).
[43]F. Diedrich, E. Peik, J. M. Chen, W. Quint, and H. Walther, Phys. Rev. Lett. **59**, 2931 (1987).
[44]D. J. Wineland, J. C. Bergquist, W. M. Itano, J. J. Bollinger, and C. H. Manney, Phys. Rev. Lett. **59**, 2935 (1987).
[45]H. Walther, Adv. At. Mol. Opt. Phys. **31**, 137 (1993).
[46]R. Rafac, J. P. Schiffer, J. S. Hangst, D. H. E. Dubin, and D. J. Wales, Proc. Natl. Acad. Sci. USA **88**, 483 (1991).
[47]J. P. Schiffer, Phys. Rev. Lett. **70**, 818 (1993).
[48]D. H. E. Dubin, Phys. Rev. Lett. **71**, 2753 (1993).
[49]D. H. E. Dubin, Phys. Rev. A **40**, 1140 (1989).
[50]R. W. Hasse and V. V. Avilov, Phys. Rev. A **44**, 4506 (1991).
[51]J. N. Tan, J. J. Bollinger, and D. J. Wineland, Bull. Am. Phys. Soc. **38**, 1972 (1993).
[52]D. Habs, in *Frontiers of Particle Beams*, Lecture Notes in Physics (Springer, New York, 1988), Vol. 296.
[53]R. W. Hasse and J. P. Schiffer, Ann. Phys. **203**, 419 (1990).
[54]U. Eichmann, J. C. Bergquist, J. J. Bollinger, J. M. Gilligan, W. M. Itano, D. J. Wineland, and M. G. Raizen, Phys. Rev. Lett. **70**, 2359 (1993).
[55]R. Hasse, Phys. Rev. A **45**, 5189 (1992).
[56]S. Chen and D. H. E. Dubin, Phys. Rev. Lett. **71**, 2721 (1993).
[57]P. Lett, R. Watts, C. Westbrook, W. D. Phillips, P. Gould, and H. Metcalf, Phys. Rev. Lett. **61**, 169 (1988).
[58]See, for example, C. Cohen-Tannoudji and W. D. Phillips, Phys. Today **43**, 33 (1990).
[59]D. J. Heinzen, J. J. Bollinger, F. L. Moore, W. M. Itano, and D. J. Wineland, Phys. Rev. Lett. **66**, 2080 (1991).
[60]M. D. Tinkle, R. G. Greaves, C. M. Surko, R. L. Spencer, and G. W. Mason, Phys. Rev. Lett. **72**, 352 (1994).

[61]C. S. Weimer, J. J. Bollinger, F. L. Moore, and D. J. Wineland, to be published in Phys. Rev. A.
[62]D. H. E. Dubin, Phys. Rev. Lett. **66**, 2076 (1991).
[63]D. H. E. Dubin, Phys. Fluids B **5**, 295 (1993).
[64]T. J. Murphy and C. M. Surko, Phys. Rev. A **46**, 5696 (1992).
[65]G. Gabrielse, X. Fei, L. A. Orozco, R. L. Tjoelker, J. Hass, H. Kalinowsky, T. A. Trainor, and W. Kells, Phys. Rev. Lett. **65**, 1317 (1990).
[66]R. Keinigs, Phys. Fluids **24**, 860 (1981); **27**, 1427 (1984).
[67]S. A. Prasad and T. M. O'Neil, Phys. Fluids **26**, 665 (1983).
[68]D. H. E. Dubin and J. P. Schiffer (private communication, 1993).
[69]P. M. Morse and H. Feshbach, *Methods of Theoretical Physics* (McGraw-Hill, New York, 1953), pp. 661–2.